Shape memory behavior and recovery force of 4D printed textile functional composites

Wei Zhang[a,b], Fenghua Zhang[c], Xin Lan[c], Jinsong Leng[c], Amanda S. Wu[d], Taylor M. Bryson[d], Chase Cotton[e], Bohong Gu[a], Baozhong Sun[a,**], Tsu-Wei Chou[b,*]

[a] College of Textiles, Donghua University, Shanghai 201620, PR China
[b] Department of Mechanical Engineering, Center for Composite Materials, University of Delaware, Newark, DE 19716, USA
[c] Center for Composite Materials and Structures, Harbin Institute of Technology, Harbin 150080, PR China
[d] Lawrence Livermore National Laboratory, CA 94550, USA
[e] Department of Electrical and Computer Engineering, University of Delaware, Newark, DE 19716, USA

A B S T R A C T

Four-dimensional (4D) printing of multi-directionally reinforced preforms has tremendous potential for the development of next generation functional composites by using the capabilities of 3D printing technology, 3D textile preform design, and polymer shape memory behavior. This work demonstrates the shape memory behavior and recovery force of 4D printed circular braided tube preforms and their silicone elastomer matrix composites. The preforms were printed by fused deposition modeling using the shape memory polymer (SMP), polylactic acid (PLA). The effects of braiding angle, tube wall thickness, and shape recovery temperature on the shape memory behavior of 4D printed tube preforms and their silicone elastomer matrix composites have been characterized. Measurements of shape recovery forces of the preform and composite were conducted using dynamic mechanical analysis (DMA). The braided microstructural parameters and shape recovery temperature have a significant effect on the preform shape memory behavior. The introduction of the silicone elastomer matrix greatly enhances the shape recovery force, shape recovery ratio, as well as radial compressive failure load of the 4D printed preform/silicone elastomer matrix composite. Building on these results, a potential application for 4D printed textile functional composites is presented.

1. Introduction

Four dimensional (4D) printing, the convergence of 3D printing and shape-morphing materials, was first introduced by Tibbits [1] in 2013 and has attracted considerable attention. It not only possesses the advantage of 3D printing that enables flexible fabrication of objects with complex shapes, but also has the capability of changing the shape, property, or functionality of 3D printed structures under external stimuli such as temperature, light, electric and magnetic field, and water [2–6]. Owing to its distinct advantages, 4D printing has been adopted in various technological fields, such as biomimetic structures [7], robotics [8], electronic devices [9], medical devices [10,11] as well as tissue engineering [12,13].

3D printing, also known as additive manufacturing, has been utilized to print numerous lightweight engineering and medical structures, such as lattices [14,15], honeycombs [16,17], scaffolds [11,18–20]and stents [21,22] with outstanding mechanical properties. For example,

Cabrera et al. [21] demonstrated the design and manufacture of a polymer stent with mechanical performance comparable to that of conventional nitinol stents used for heart valve implantation in animal trials. Morrison et al. [23] designed and printed a tracheo-bronchomalacia splint for personalized medical device. Prates [24] presented a customized and lightweight, waterproof, ventilated 3D printed multi-material cervical orthosis.

Shape memory polymer (SMP), as one of the most widely used smart materials, has been adopted for 4D printing. For example, Yang et al. [25] developed a photoresponsive shape memory composite based on shape memory polymers and carbon black with high photothermal conversion efficiency. Yu et al. [26] synthesized a shape memory epoxy-acrylate hybrid photopolymer to fabricate complex structures through a stereolithography 3D printing technique. Ge et al. [27] developed a 4D printing approach that can create multimaterial SMP architectures using a family of photo-curable methacrylate based copolymer networks. Ly et al. [28] investigated the properties of shape

---

memory polyurethane and its CNT composites. Zarek et al. [9] developed a type of SMP based on polycaprolactone (PCL) and used it for flexible electronic devices. Zhao et al. [29] demonstrated the shape memory behavior of 3D printed objects with FDM using shape memory zinc-neutralized poly(ethylene-comethacrylic acid). Apart from above the mentioned SMP materials, polylactic acid (PLA) is also a well-known SMP, which has been used in the biomedical field because of its good biodegradability and biocompatibility [30,31]. Senatov et al. [19], for example, has developed a 3D printed porous shape memory scaffold based on PLA/15% wt. nano-hydroxyapatite (HA) for self-fitting implants.

3D textile structural preforms, as the reinforcing phase of advanced composites, possess the unique characteristics of multi-directional reinforcement, improved structural integrity as well as flexible microstructural designability [32]. Quan et al. have successfully printed some 3D braided, orthogonal and interlock preforms, and composites [33–36]. By using the capabilities of 3D printing technology, 3D textile preform design, as well as polymer shape memory, 4D printing of multi-directional reinforced preforms has tremendous potential for the development of next generation functional composites. Here, the 4D printed braided tube preforms were designed and fabricated by fused deposition modeling using SMP PLA filament. The 4D printed braided tube/silicone elastomer composites were also fabricated to enhance shape memory effects and mechanical properties. The shape memory behaviors and radial compression properties of 4D printed circular braided tube preforms and composites were characterized. The effects of braiding angle, wall thickness of the preforms, as well as the shape recovery temperature on the specimen shape memory behaviors were studied. The thermomechanical properties and shape recovery force were measured using a dynamic mechanical analysis.

2. Experimental section

2.1. Materials and thermal properties test

The SMP PLA filaments provided by Harbin Institute of Technology (HIT) were used for fabrication of 4D printed circular braided tube preform. To understand the thermal properties of SMP PLA filaments, the Differential scanning calorimetry (DSC) was conducted under nitrogen atmosphere using a Discovery DSC (TA Instruments). The sample weight was around 5 mg. The ramp rate was 10 °C/min. The thermal gravimetric analysis (TGA) was also conducted under nitrogen atmosphere using Discovery TGA (TA Instruments) with the same ramp rate of 10 °C/min. The sample weight was around 10 mg.

2.2. Specimen fabrication

The microstructure models used for 3D printing of the circular braided tube preforms were established by the software of CATIA. Based on the established microstructure models, 3D circular braided tube preforms with three braiding angles (20°, 30° and 40°) and three wall thicknesses (two layers, three layers and five layers) were printed by fused deposition modeling (FDM) using the SMP PLA filament. The printer nozzle temperature was 200 °C and printing speed was 40 mm/s. The layer thickness was 0.2 mm. All preforms were printed using a QIDI Tech dual-nozzle 3D printer (Qidi Technology Co., Ltd., Ruian, Zhejiang, China). 4D printed circular braided tube preform/silicone elastomer matrix composite was fabricated by infusing the tubular preforms with a silicone elastomer matrix (184 silicone elastomer system, Dow Corning Inc., Michigan, U.S.). Vacuum was applied to eliminate the air in the silicone system. To avoid the effect of elevated temperature on the shape memory polymer preforms, the silicone elastomer matrix composites were cured in room temperature for 48 h. The PLA polymer's volume fraction in the composite was calculated as 36% by measuring the volume of the preform and composite, respectively. A video camera (Sony FDR-AX100) was used to obtain the

images of the preform and the composite. A stereo microscope with integrated HD USB camera (Mantis Elite-Cam HD) was used to obtain the enlarged optical image of preform surface.

2.3. Shape memory behavior characterization

The shape memory behaviors of 4D printed circular braided tube preform and the preform/silicone elastomer matrix composite were characterized. The predeformed intermediate shape specimen was put in an oven with the given recovery temperature above the printing filament's glass transition temperature. A video camera (Sony FDR-AX100) was used to record the shape recovery process. The effects of braiding angle, tube wall thickness and recovery temperature on the shape memory behavior were investigated.

2.4. Thermomechanical properties and shape recovery force measurement

The dynamic thermomechanical analysis and shape recovery force of the 4D printed circular braided tube preform and the preform/silicone elastomer matrix composite at the intermediate shape were conducted using the RSA-G2 DMA (TA Instruments) with compressive oscillatory temperature ramp from 25 °C to 90 °C with the ramp rate of 5 °C/min. We applied a 1g force prior to starting the test to ensure contact with the sample and set the constant strain to 0.1%. The frequency was 1Hz. The type of loading was compressive-compressive. The storage modulus, loss modulus, Tan delta and shape recovery force were obtained.

2.5. Radial compression test

Following the ASTM-D2412 standard [37], radial compression tests of 4D printed circular braided tube preforms and composites were carried out on an Instron universal testing machine equipped with a 500 N load cell. All tests were run at the loading rate of 12.7 mm/min. Three specimens of each type were loaded until failure or crush. The fracture surface morphology of the specimens was examined using an Auriga 60 scanning electron microscope (SEM) at an accelerating voltage of 3.0 kV.

3. Results and discussion

The 4D printed circular braided tube preform was fabricated by fused deposition modeling. Fig. 1(a)–(c) show the 3D braided microstructure. From the braiding yarn contour projection in Fig. 1(a), it can be seen that each yarn traverses from one surface to the other through the tube thickness. Fig. 1(b) shows the unit cell model, which is composed of three parts, namely, outer surface, interior and inner surface. The interior part has four interlaced yarns; each surface part has two yarns. The repeating unit cells constitute the whole geometrical model, as shown in Fig. 1(c). Here, α denotes the braiding angle, a key structural parameter of the braided preform. In order to analyze the effects of microstructural parameters on the shape memory behavior of 4D printed circular braided tubes, models of three braiding angles (20°, 30° and 40°) as well as three braided tube wall thicknesses (two, three and five layers) were established.

Differential scanning calorimetry (DSC) and thermal gravimetric analysis (TGA) measurements were conducted to characterize the thermal properties of the SMP PLA filament. It can be seen from Fig. 1(d) that the glass transition temperature (Tg) of the filament was around 63 °C; the crystallization temperature and melting temperature were around 110 °C and 170 °C, respectively. The Tg, crystallization temperature and melting temperature are very similar to those temperatures of PLA in the literature [19]. Fig. 1(e) shows that the degradation temperature was around 345 °C. Based on the measured thermal properties of SMP PLA filament, the 3D printer nozzle temperature was chosen to be 200 °C. In the subsequent characterization of
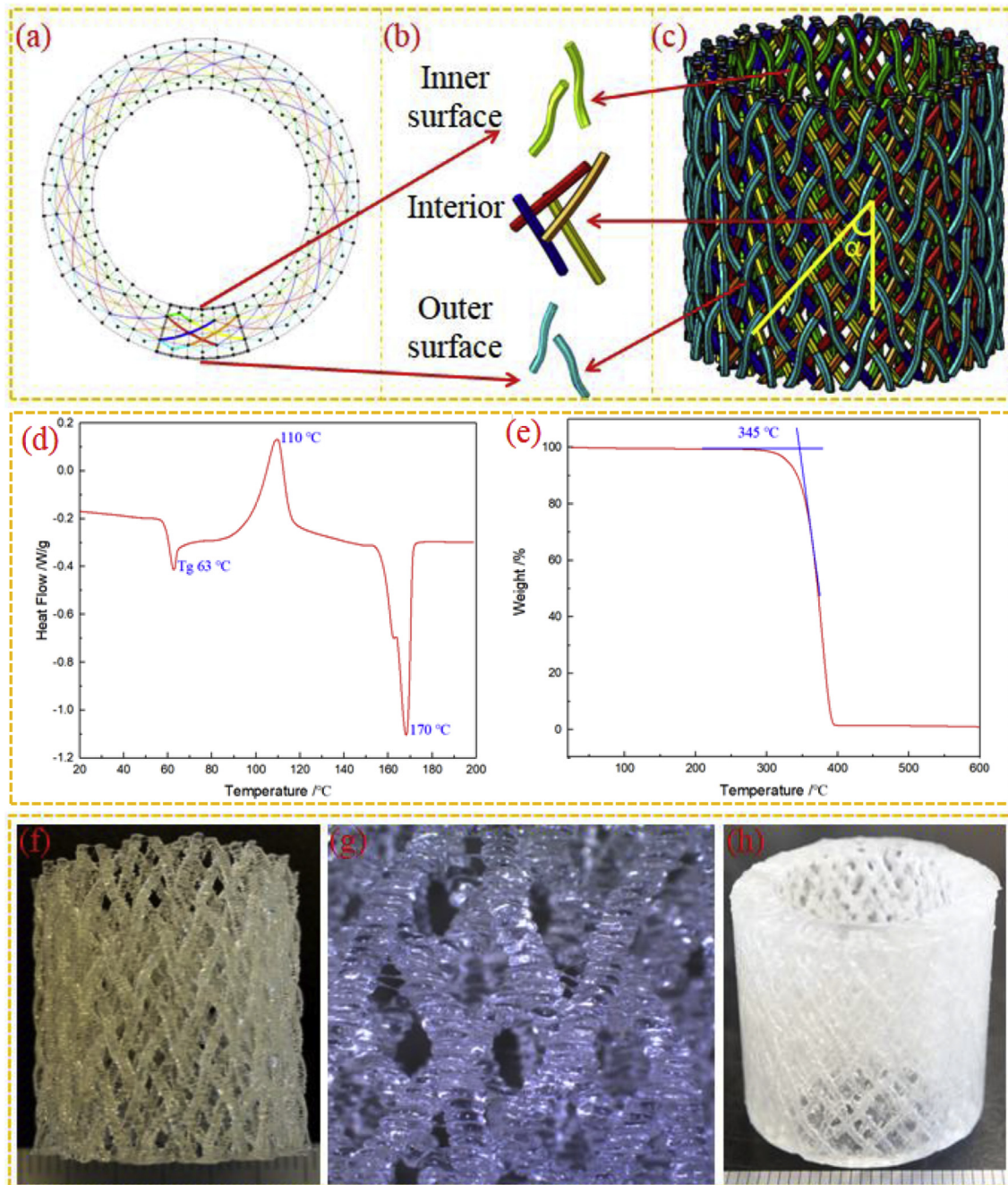
Fig. 1. 3D circular braided tube model and specimens with braiding angle of 30° and three braiding layers: (a) yarn contour projection, (b) unit cell model, (c) tube geometrical model, (d) DSC curve and (e) TGA curve of SMP PLA filaments for 4D printing, (f) 4D printed circular braided tube preform, (g) enlarged optical image of preform surface and (h) 4D printed circular braided tube preform/silicone elastomer matrix composite.

shape memory behavior, the deformation temperature (T_d) during mechanical loading was selected to be 90 °C and the shape recovery temperatures (T_r) were 70 °C, 80 °C and 90 °C.

Based on the geometrical model design and the SMP PLA filament, 3D circular braided tube preforms were printed by fused deposition modeling. Fig. 1(f) shows a printed preform with the braiding angle of 30° and three braiding layers. The tube height is around 24 mm. The outer diameter and inner diameter of the tube are around 25 mm and 18.4 mm, respectively. Fig. 1(g) shows the enlarged preform surface optical image. In this study, tube preforms with three braiding angles (20°, 30° and 40°) and three braided tube thicknesses (two, three and five layers) were printed. Composites based on 4D printed circular braids were fabricated by infusing the tubular preforms with a silicone

elastomer matrix. Fig. 1(h) shows a 4D printed circular braided tube preform/silicone elastomer matrix composite with the braiding angle of 30° and three braiding layers.

The shape memory behavior of 4D printed circular braided tubes has been characterized following the procedure shown in Fig. 2(a). First, the as-printed specimen (Fig. 2(a1)) was deformed to an intermediate shape under external load at T_d in an oven. This intermediate shape was maintained when the specimen was cooled down to the room temperature and unloaded. Finally, the specimen recovered to nearly its original shape upon heating at T_r above its glass transition temperature, and the shape memory cycle was complete. A video camera was used to record the shape recovery process. According to the recorded images, the shape recovery ratio, $R_{r,t}$, at recovery time t, was calculated using
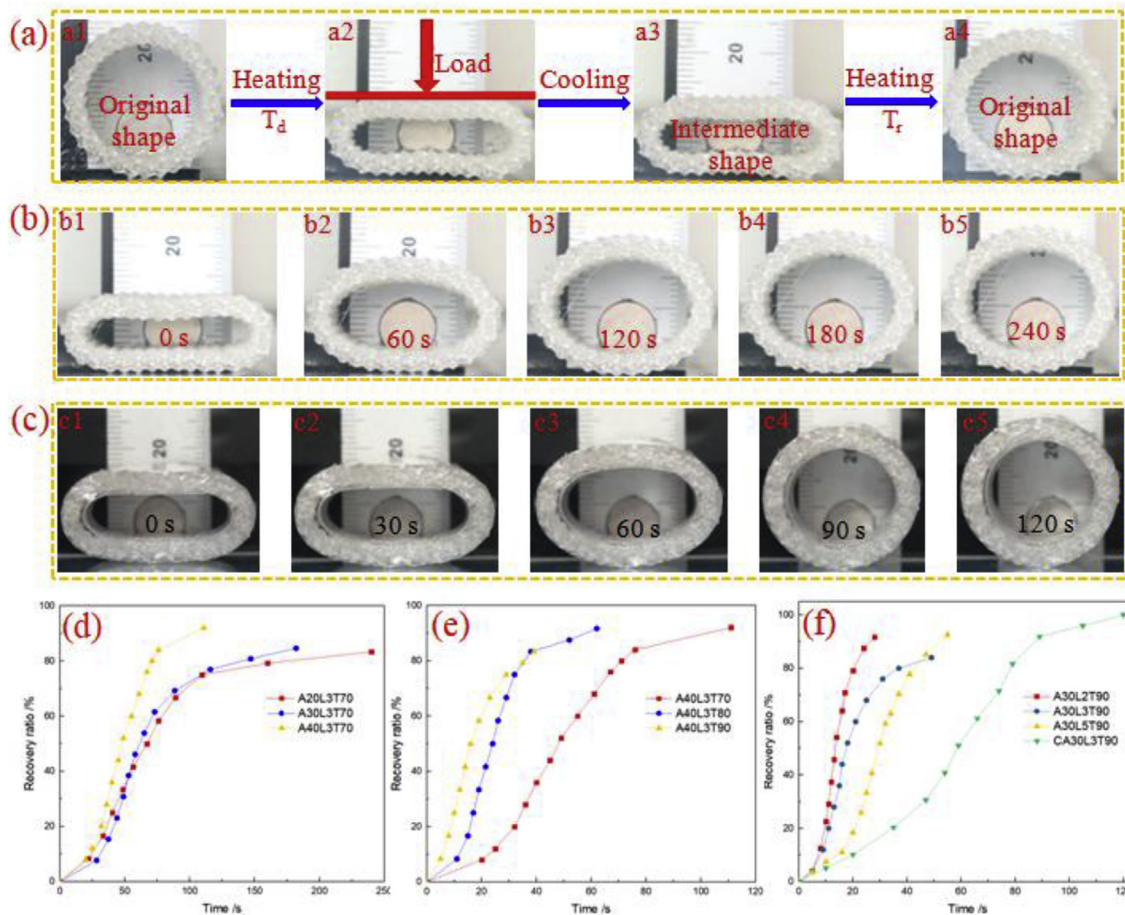
Fig. 2. (a) Shape memory cycle of 4D printed circular braided tube, (b) shape recovery of the specimen A30L3T70, (c) shape recovery of specimen CA30L3T90, (d) shape recovery ratio vs. time curves of specimens L3T70 with three braiding angles of 20°, 30° and 40°, (e) shape recovery ratio vs. time curves of specimens A40L3 at three shape recovery temperatures of 70 °C, 80 °C and 90 °C, as well as (f) shape recovery ratio vs. time curves of specimens A30T90 with two braiding layers, three braiding layers and five braiding layers and the specimen CA30L3T90. (Notes: the legends A, L and T denote the braiding angle, braiding layer and recovery temperature, respectively. C denotes composite specimen, and the legend without C means the preform. For instance, A20L3T70 denotes the preform with braiding angle of 20° and three braiding layers at the recovery temperature of 70 °C.)

the equation $R_{r.t}(\%) = \frac{(h_t - h_i)}{(h_o - h_i)} \times 100$, where the h_o, h_t and h_i denote, respectively, the tube cross-sectional height of the original state, at time t, and the intermediate state. Fig. 2(b) shows the time variation of shape recovery of 4D printed braided tube preform with the braiding angle of 30° and three braiding layers at the shape recovery temperature of 70 °C. The specimen readily recovers to nearly its original shapes in 240 s. Fig. 2(c) shows the time variation of shape recovery of 4D printed braided tube preform/silicone elastomer matrix composite with the braiding angle of 30° and three braiding layers at the shape recovery temperature of 90 °C. The composite completely recovers to its original shape in 120 s. The effects of braiding angle, shape recovery temperature and tube wall thickness on the preform shape memory behavior have also been characterized. Fig. 2(d) shows shape recovery ratio vs. time curves of 4D printed circular braided tube preforms with three braiding angles of 20°, 30° and 40° at the same wall thickness of three layers and shape recovery temperature of 70 °C. The S-shaped curves all show lower recovery rate at the initial and final stages, and majority of the recovery is accomplished in the middle stage. The recovery rate of 40° specimen is higher than those 20° and 30° specimens. The final recovery ratios of the 20°, 30° and 40° specimens are around 83.3%, 84.6% and 92%, respectively. These results could be attributed to the fact that there is higher degree of circumferential reinforcement as braiding angle increases. Fig. 2(e) shows the shape recovery ratio vs. time curves of 4D printed braided tube preforms with the same braiding angle of 40° and wall thickness of three layers at three shape recovery

temperatures of 70 °C, 80 °C and 90 °C. All the specimens recover to most of their original shapes in 120 s. The shape recovery rate increases with increasing recovery temperature. The final shape recovery ratios of the specimens at the three recovery temperatures of 70 °C, 80 °C and 90 °C are, respectively, 92%, 91.7% and 83.3%, which decrease with increasing recovery temperature. Fig. 2(f) shows the shape recovery ratio vs. time curves of 4D printed braided tube preforms with two braiding layers, three braiding layers and five braiding layers and the composite of three braiding layers at the same braiding angle of 30° and shape recovery temperature of 90 °C. It can be seen that the preform shape recovery time increases in the order of two-layers, three-layers and five-layers. The preform with two braiding layers shows the fastest shape recovery rate. The final shape recovery ratios of the preforms of two-layers, three-layers and five-layers are, respectively, 91.5%, 84% and 92.6%. Compared with the recovery ratio of 84% for the corresponding preform at the same recovery temperature, the recovery ratio of silicone elastomer matrix composite was improved markedly with the final shape recovery ratio of 100%. The increased shape recovery time of the composite increased is attributed to the low thermal conductivity of the silicone elastomer.

In order to better understand the shape recovery capability of the 4D printed circular braided tube preform and its silicone elastomer matrix composite, their shape recovery forces were measured. Fig. 3(a) shows the variation of thermomechanical properties and recovery force of the tube preform from 25 °C to 90 °C measured with DMA
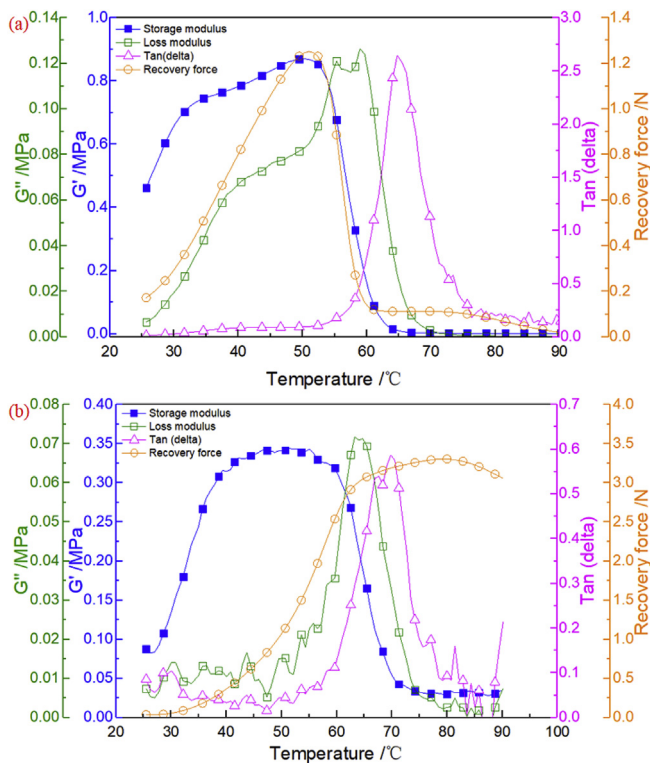
Fig. 3. Thermomechanical properties and recovery force of (a) 4D printed circular braided tube preform and (b) 4D printed circular braided tube preform/silicone elastomer matrix composite.

compressive oscillatory temperature ramp. The Tan (delta) reaches its peak value at 65 °C, which is considered as the glass transition temperature of the preform. This value is close to the glass transition temperature of the 4D printing PLA filament measured by DSC. The storage modulus rapidly decreases in the glass transition region from 50 °C to 65 °C and the specimen exhibits a low modulus at temperatures above 65 °C. The recovery force increases with increasing temperature and reaches to its peak value of 1.25 N at 51 °C, and then the recovery force rapidly decreases to about 0.11 N in the glass transition region (50 °C–63 °C). This is consistent with the result of storage modulus. After that, the recovery force keeps a stable level between 63 °C and 75 °C and then decreases to 0.02 N with increasing temperature up to 90 °C.

Fig. 3(b) shows the variation of thermomechanical properties and recovery force of 4D printed circular braided tube preform/silicone elastomer matrix composite from 25 °C to 90 °C. It can be seen from the peak value of Tan (delta) that the glass transition temperature of the composite is around 70 °C, which is slightly higher than that of the preform. The storage modulus rapidly decreases in the glass transition region from 50 °C to 70 °C and the specimen exhibits a low modulus at temperatures above 70 °C. The recovery force gradually increases with increasing temperature from 25 °C to 50 °C. After that, in the glass transition region, the recovery force rapidly increases with increasing temperature and reaches the peak value of 3.3 N at 80 °C, which is much larger than that of the preform. This result confirms that the introduction of the matrix material results in the high recovery force of 4D printed circular braided tube preform/silicone elastomer composite. Furthermore, the 4D printed composite shows a much wider temperature application range compared with its braided tube preform.

The failure behavior of 4D printed preforms and composites was studied using radial compression. Fig. 4(a) shows the five stages of failure progression of the circular braided tube preform with the braiding angle of 40° and three braiding layers; their corresponding load-displacement data are marked in Fig. 4(b), which gives the load-

radial displacement curves of preforms with braiding angles of 20°, 30° and 40° at the same wall thickness. The maximum load at specimen compressive failure increases with increasing braiding angle. This is mainly because there is higher degree of circumferential reinforcement as braiding angle increases; this is consistent with the result of shape recovery ratio. The tube radial displacement corresponding to the maximum load decreases with increasing braiding angle. Fig. 4(c) shows the load-displacement curves of the preforms with two, three and five braiding layers at the same braiding angle of 30°. The maximum load at compressive failure increases with increasing braiding layer. The load-displacement curves of the preform and silicone elastomer matrix composite were compared in Fig. 4(d). It can be seen that the maximum load at compressive failure is much larger than that of the preform. The displacement corresponding to the maximum load of the composite is also larger than that of the preform. In addition, the irregular broken lines in the load-radial displacement curves of the preforms and composite indicate that the breakages of the printed wires in the braided structure preforms were not simultaneous. The fracture images in different positions also showed this point. Fig. 4(e)–(g) shows the SEM images of radial compressive failure of 4D printed circular braided tube preforms. It can be seen that the printed spiral wires interlaced together. The breakage occurs not only at the interface between printed layers, as shown in Fig. 4(e), but also in the wire, as shown in Fig. 4(f). Fig. 4(g) shows multiple yarn breakages.

The 4D printed circular braided tube preform/silicone elastomer matrix composite possesses not only excellent recovery capability in the radial direction, but also remarkable circumferential recovery ability from an unfolded state. To demonstrate the potential functional application of the 4D printed composites as mechanical grippers, the circumferential recovery capability of the braided tube is utilized. Here, an "open" composite tube specimen was first fabricated by cutting the composite tube along its longitudinal direction, and then flattened to assume the unfolded state. Fig. 5 shows the shape memory behavior of an open 4D printed braided tube preform/silicone elastomer matrix composite with the braiding angle of 30° and three braiding layers at the shape recovery temperature of 70 °C. At this relatively low recovery temperature, the unfolded specimen recovered to nearly its original tubular shape during the recovery time of 250s. The shape recovery ratio was almost 100%.

4. Conclusions

In this research, 4D printed circular braided tube preforms and their silicone elastomer matrix composites were accomplished and a shape memory investigation was performed. The shape memory behaviors were primarily influenced by the microstructural parameters (braiding angle and wall thickness) and the shape recovery temperature. Compared with the 4D printed circular braided tube preform, the introduction of a silicone elastomer not only significantly improved the radial compressive failure load of the 4D printed tube preform/silicone elastomer matrix composite, but also markedly enhanced the shape recovery force at a wider operation temperature range, resulting in full shape recovery. The remarkable shape memory behavior and mechanical properties as well as flexibility in microstructural design confirm the potential of functional applications of 4D printing of textile composites. The example of a mechanical gripper has been demonstrated.
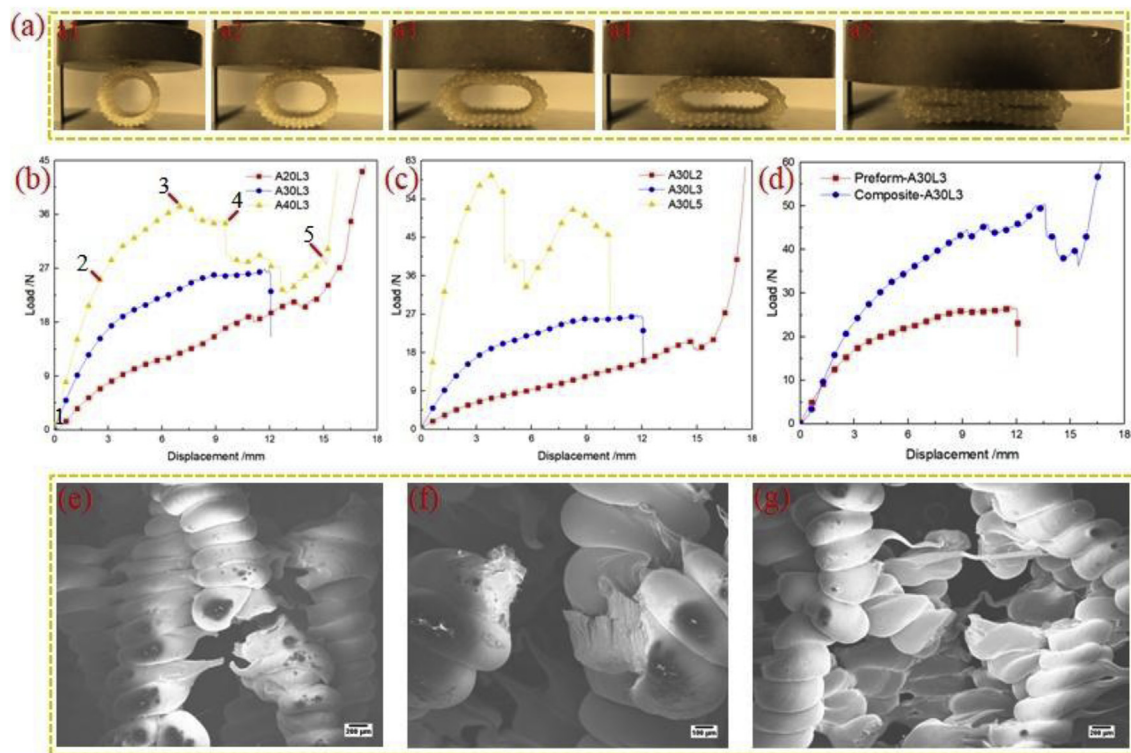
Fig. 4. 4D printed circular braided tube preform (a) radial compressive failure process, and load vs. displacement curves at (b) three braiding angles of 20°, 30° and 40°, (c) three wall thicknesses of two, three and five layers, (d) comparison of load vs. displacement curves of the preform and silicone elastomer matrix composite, and (e)-(g) SEM images of specimen failure.
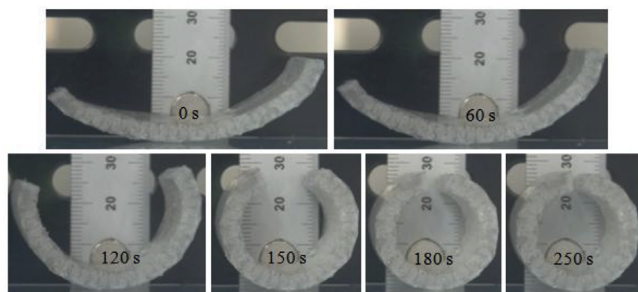

Fig. 5. Shape memory behavior of an open 4D printed braided tube preform/ silicone elastomer matrix composite with the braiding angle of 30° and three braiding layers at the shape recovery temperature of 70 °C.

Appendix A. Supplementary data

Supplementary data related to this article can be found at http://dx. doi.org/10.1016/j.compscitech.2018.03.037.

References

[1] S. Tibbits, The emergence of "4D printing", TED Talk, 2013.

[2] F. Momeni, S.M. Mehdi Hassani, N.X. Liu, J. Ni, A review of 4D printing, Mater. Des. 122 (2017) 42–79.

[3] J. Choi, O.C. Kwon, W. Jo, H.J. Lee, M.-W. Moon, 4D printing technology: a review, 3D Print. Addit. Manuf. 2 (4) (2015) 159–167.

[4] D.-G. Shin, T.-H. Kim, D.-E. Kim, Review of 4D printing materials and their properties, Int. J. Precis. Eng. Manuf.-Green Tech 4 (3) (2017) 349–357.

[5] J. Lee, H.-C. Kim, J.-W. Choi, I.H. Lee, A review on 3D printed smart devices for 4D printing, Int. J. Precis. Eng. Manuf.-Green Tech 4 (3) (2017) 373–383.

[6] Y. Zhou, W.M. Huang, S.F. Kang, X.L. Wu, H.B. Lu, J. Fu, H. Cui, From 3D to 4D printing: approaches and typical applications, J. Mech. Sci. Technol. 29 (10) (2015) 4281–4288.

[7] A.S. Gladman, E.A. Matsumoto, R.G. Nuzzo, L. Mahadevan, J.A. Lewis, Biomimetic 4D printing, Nat. Mater. 15 (4) (2016) 413–418.

[8] M. Lopez-Valdeolivas, D. Liu, D.J. Broer, C. Sanchez-Somolinos, 4D printed

actuators with soft-robotic functions, Macromol. Rapid Commun. (2017), http://dx. doi.org/10.1002/marc.201700710.

[9] M. Zarek, M. Layani, I. Cooperstein, E. Sachyani, D. Cohn, S. Magdassi, 3D printing of shape memory polymers for flexible electronic devices, Adv. Mater 28 (22) (2016) 4449–4454.

[10] M. Zarek, N. Mansour, S. Shapira, D. Cohn, 4D printing of shape memory-based personalized endoluminal medical devices, Macromol. Rapid Commun. 38 (2) (2017).

[11] D. Liu, T. Xiang, T. Gong, T. Tian, X. Liu, S. Zhou, Bioinspired 3D multilayered shape memory scaffold with a hierarchically changeable micropatterned surface for efficient vascularization, ACS Appl. Mater. Interfaces 9 (23) (2017) 19725–19735.

[12] S. Miao, N. Castro, M. Nowicki, L. Xia, H. Cui, X. Zhou, W. Zhu, S.-j. Lee, K. Sarkar, G. Vozzi, Y. Tabata, J. Fisher, L.G. Zhang, 4D printing of polymeric materials for tissue and organ regeneration, Mater. Today 20 (10) (2017) 577–591.

[13] W.J. Hendrikson, J. Rouwkema, F. Clementi, C.A. van Blitterswijk, S. Fare, L. Moroni, Towards 4D printed scaffolds for tissue engineering: exploiting 3D shape memory polymers to deliver time-controlled stimulus on cultured cells, Biofabrication 9 (3) (2017) 031001.

[14] S. Liu, Y. Li, N. Li, A novel free-hanging 3D printing method for continuous carbon fiber reinforced thermoplastic lattice truss core structures, Mater. Des. 137 (2018) 235–244.

[15] Q. Chen, J.D. Mangadlao, J. Wallat, A. De Leon, J.K. Pokorski, R.C. Advincula, 3D printing biocompatible polyurethane/poly(lactic acid)/graphene oxide nano-composites: anisotropic properties, ACS Appl. Mater. Interfaces 9 (4) (2017) 4015–4023.

[16] Y. Chen, T. Li, Z. Jia, F. Scarpa, C.-W. Yao, L. Wang, 3D printed hierarchical hon-eycombs with shape integrity under large compressive deformations, Mater. Des. 137 (2018) 226–234.

[17] Y. Yap, W. Yeong, Shape recovery effect of 3D printed polymeric honeycomb: this paper studies the elastic behaviour of different honeycomb structures produced by PolyJet technology, Virtual Phys. Prototyp. 10 (2) (2015) 91–99.

[18] C. Deng, Q. Yao, C. Feng, J. Li, L. Wang, G. Cheng, M. Shi, L. Chen, J. Chang, C. Wu, 3D printing of bilineage constructive biomaterials for bone and cartilage re-generation, Adv. Funct. Mater. 27 (36) (2017) 1703117.

[19] F.S. Senatov, M.Y. Zadorozhnyy, K.V. Niaza, V.V. Medvedev, S.D. Kaloshkin, N.Y. Anisimova, M.V. Kiselevskiy, K.-C. Yang, Shape memory effect in 3D-printed scaffolds for self-fitting implants, Eur. Polym. J. 93 (2017) 222–231.

[20] S. Miao, W. Zhu, N.J. Castro, M. Nowicki, X. Zhou, H. Cui, J.P. Fisher, L.G. Zhang, 4D printing smart biomedical scaffolds with novel soybean oil epoxidized acrylate, Sci. Rep. 6 (2016) 27226.

[21] M.S. Cabrera, B. Sanders, O.J.G.M. Goor, A. Driessen-Mol, C.W.J. Oomens, F.P.T. Baaijens, Computationally designed 3D printed self-expandable polymer stents with biodegradation capacity for minimally invasive heart valve implanta-tion: a proof-of-concept study, 3D Print. Addit. Manuf. 4 (1) (2017) 19–29.

[22] G.Z. Cheng, E. Folch, A. Wilson, R. Brik, N. Garcia, R.S.J. Estepar, J.O. Onieva, S. Gangadharan, A. Majid, 3D printing and personalized airway stents, Pulmonary Therapy 3 (1) (2017) 59–66.

[23] R.J. Morrison, S.J. Hollister, M.F. Niedner, M.G. Mahani, A.H. Park, D.K. Mehta, R.G. Ohye, G.E. Green, Mitigation of tracheobronchomalacia with 3D-printed personalized medical devices in pediatric patients, Sci. Transl. Med. 7 (285) (2015) 285ra64.

[24] A. Prates, Self-adjusting Orthoses Design, Scripta-Ingenia (2014).

[25] H. Yang, W.R. Leow, T. Wang, J. Wang, J.C. Yu, K. He, D.P. Qi, C.J. Wan, X.D. Chen, 3D printed photoresponsive devices based on shape memory composites, Adv. Mater 29 (33) (2017).

[26] R. Yu, X. Yang, Y. Zhang, X. Zhao, X. Wu, T. Zhao, Y. Zhao, W. Huang, Three-dimensional printing of shape memory composites with epoxy-acrylate hybrid photopolymer, ACS Appl. Mater. Interfaces 9 (2) (2017) 1820–1829.

[27] Q. Ge, A.H. Sakhaei, H. Lee, C.K. Dunn, N.X. Fang, M.L. Dunn, Multimaterial 4D printing with tailorable shape memory polymers, Sci. Rep. 6 (2016) 31110.

[28] S.T. Ly, J.Y. Kim, 4D printing–fused deposition modeling printing with thermal-responsive shape memory polymers, Int. J. Precis. Eng. Manuf.-Green Tech 4 (3) (2017) 267–272.

[29] Z. Zhao, F. Peng, K.A. Cavicchi, M. Cakmak, R.A. Weiss, B.D. Vogt, Three-dimensional printed shape memory objects based on an olefin ionomer of zinc-neutralized poly(ethylene-co-methacrylic acid), ACS Appl. Mater. Interfaces 9 (32) (2017) 27239–27249.

[30] N.C. Goulbourne, H.E. Naguib, J.J. Song, I. Srivastava, J. Kowalski, H.E. Naguib, Fabrication and Characterization of a Foamed Polylactic Acid (PLA)/Thermoplastic Polyurethane (TPU) Shape Memory Polymer (SMP) Blend for Biomedical and Clinical Applications vol. 9058, (2014) 90580B.

[31] M. Barmouz, A. Hossein Behravesh, Shape memory behaviors in cylindrical shell PLA/TPU-cellulose nanofiber bio-nanocomposites: analytical and experimental assessment, Composites Part A 101 (2017) 160–172.

[32] A. Mouritz, M. Bannister, P. Falzon, K. Leong, Review of applications for advanced three-dimensional fibre textile composites, Composites Part A 30 (12) (1999) 1445–1461.

[33] Z. Quan, A. Wu, M. Keefe, X. Qin, J. Yu, J. Suhr, J.-H. Byun, B.-S. Kim, T.-W. Chou, Additive manufacturing of multi-directional preforms for composites: opportunities and challenges, Mater. Today 18 (9) (2015) 503–512.

[34] Z. Quan, Z. Larimore, X. Qin, J. Yu, M. Mirotznik, J.-H. Byun, Y. Oh, T.-W. Chou, Microstructural characterization of additively manufactured multi-directional preforms and composites via X-ray micro-computed tomography, Compos. Sci. Technol. 131 (2016) 48–60.

[35] Z. Quan, Z. Larimore, A. Wu, J. Yu, X. Qin, M. Mirotznik, J. Suhr, J.-H. Byun, Y. Oh, T.-W. Chou, Microstructural design and additive manufacturing and characterization of 3D orthogonal short carbon fiber/acrylonitrile-butadiene-styrene preform and composite, Compos. Sci. Technol. 126 (2016) 139–148.

[36] Z. Quan, J. Suhr, J. Yu, X. Qin, C. Cotton, M. Mirotznik, T.-W. Chou, Printing direction dependence of mechanical behavior of additively manufactured 3D preforms and composites, Compos. Struct. 184 (2018) 917–923.

[37] ASTM D2412-02, Standard Test Method for Determination of External Loading Characteristics of Plastic Pipe by Parallel-plate Loading, ASTM International, West Conshohocken, PA, 2002.